NASA Technical Memorandum 82842

Pressure Transfer Function of a JT15D Nozzle Due to Acoustic and Convected Entropy Fluctuations

J. H. Miles
Lewis Research Center
Cleveland, Ohio

Prepared for the
One hundred third Meeting of the Acoustical Society of America
Chicago, Illinois, April 26–30, 1982

NASA

TRANSFER FUNCTION OF A JT15D NOZZLE DUE TO ACOUSTIC AND CONVECTED ENTROPY FLUCTUATIONS

by

J. H. Miles

National Aeronautics and Space Administration

Lewis Research Center

Cleveland, Ohio

ABSTRACT

An acoustic transmission matrix analysis of sound propagation in a variable area duct with and without flow is extended to include convected entropy fluctuations. The boundary conditions used in the analysis are a transfer function relating entropy and pressure at the nozzle inlet and the nozzle exit impedance. The nozzle pressure transfer function calculated with this analysis is compared with JT15D turbofan engine nozzle data. The one dimensional theory for sound propagation in a variable area nozzle with flow but without convected entropy is good at the low engine speeds where the nozzle exit Mach number is low (M=0.2) and the duct exit impedance model is good. The effect of convected entropy appears to be so negligible that it is obscured by the inaccuracy of the nozzle exit impedance model, the lack of information on the magnitude of the convected entropy and its phase relationship with the pressure, and the scatter in the data. It appears an improved duct exit impedance model is required at the higher engine speeds where the nozzle exit Mach number is high (M=0.56) and at low frequencies (below 120 Hz). Nevertheless, the results show the one dimensional sound propagation model does apply to the JT15D turbofan engine nozzle data.

E-1212

NOMENCLATAURE

$\mathcal{A}$	matrix
A	area, m^2
c_o	isentropic speed of sound, m/s
c_p	gas specific heat at constant pressure, J/kg K
c_v	gas specific heat at constant volume, J/kg K
f	frequency, Hz
i	$(-1)^{1/2}$
k	wave number, ω/c, m^{-1}
L	duct length, m
M_o	Mach number
(MW)	gas molecular weight
m	d ln(A)/dx, m^{-1}
P	transformation matrix
p	pressure, Pa
R	gas constant, J/kg K
S	temperature power spectral density, K^2/Hz
s	entropy, J/kg K
T	transmission matrix
t	time, s
u	velocity, m/s
x	Cartesian coordinate, m
Y	acoustic state vector
Z	acoustic impedance, mks Rayles
γ	gas specific heat ratio
Δx	region length, m
λ	eigenvalue

ρ gas density, kg/m^3

θ temperature, K

ω angular frequency, radians/s

Superscripts and subscripts:

o reference state quantity

1 perturbed quantity

INTRODUCTION

Internally generated turbojet engine noise is important at low power settings where the core noise level usually exceeds that of the pure jet noise. This noise can be attributed to several sources, such as combustion, turbulence in the turbine or nozzle, and flow incidence upon struts.

The combustion process produces two noise generation effects. The first can be attributed to the fluctuating heat release rate which produces isentropic pressure waves that propagate through the engine and are radiated to the far field. The second can be attributed to local regions of hot gas (entropy variations) which convect through the engine with the mean flow. The entropy variations are not a direct noise source since they have no associated pressure disturbance. However, as the entropy convects through regions with area variations acoustic waves are generated. Furthermore, the isentropic pressure waves generated by the combustion process also interact with area variations. The resulting waves represent a combination of waves due to both sources of change.

As part of a core noise research program conducted at the NASA Lewis Research Center, far field and internal pressure measurements were made near the entrance and exit of a JT15D core exit nozzle over a range of engine power settings (Ref. 1). Using these measurements nozzle pressure transfer

functions were calculated. Similar data for the YF102 turbofan engine were available. However, the core nozzle exit and inlet areas of the YF102 are nearly equal while the exit area of the JT15D core nozzle is half the inlet area. Since an entropy perturbation must convect through an area channge to produce an acoustic pressure, only the JT15D data are used herein.

In this report, first the acoustic transmission matrix approach developed in Ref. 2 to study isentropic sound propagation through a variable area duct or nozzle carrying a compressible subsonic flow is extended to include convected entropy effects. Then this analytical propagation model is used to calculate a nozzle exit pressure transfer function. Last, the measured and calculated nozzle pressure transfer functions are compared.

BACKGROUND

Entropy noise is one of the many sources of excess noise reviewed by Ffowcs Williams in Ref. 3. Many studies of noise due to entropy convecting through area changes have been made. The problem of noise production due to convected entropy fluctuations in a choked nozzle was studied theoretically by Candel (Ref. 4) and Marble and Candel (Ref. 5). Noise production by this mechanism in a subsonic nozzle was studied theoretically by Bohn (Ref. 6), Lu (Ref. 7), and Ffowcs Williams and Howe (Ref. 8). Entropy noise has been studied experimentally by Zukoski and Auerback (Ref. 9), Auerback (Ref. 10), Bohn (Ref. 11), Strahle, et al. (Ref. 12), and Muthukrishnan, et al. (Ref. 13). A brief but comprehensive review of the early work is given in Ref. 5.

Noise production by entropy fluctuations passing through turbines of current aircraft engines has been studied by Pickett (Ref. 14) and Cumpsty and Marble (Refs. 15 and 16).

The governing equations applied herein were originally used by Tsien (Ref. 17) and Crocco and Cheng (Ref. 18) to study combustion instability in a rocket

combustion chamber. The approach taken herein is to decompose the entropy inhomogeneity into a Fourier distribution of entropy variations. These equations and this approach also were used in Refs. 4 tc 7.

In the study of noise due to convected entropy fluctuations, Candel (Ref. 4), Candel and Marble (Ref. 5) and Bohm (Ref. 6) introduce the assumption of linear mean velocity distributions in the nozzle used by Tsien (Ref. 17) which allows some analytical simplifications. The theoretical study of this problem was simplified by Lu (Ref. 7) when he used an exponential nozzle in formulating his entropy noise model. The analysis presented herein is more general since it is applicable to arbitrary nozzle shapes and velocity profiles. Furthermore, it is simple to use and yields results directly comparable with measurements.

In this paper, the governing equations are derived by linearizaton and put into state variable form using acoustic pressure, particle velocity, and entropy as the state variables. Then, in order to solve the resulting differential equations, the nozzle is divided into regions in which the coefficients of the differential equation can be made constant by assuming an exponential area variation. A transmission matrix is obtained for each region by solving the acoustic state variable differential equation using the eigenvector matrix exponential method described by Ogata (Ref. 19). Other procedures for computing the exponential of a matrix are reviewed in Ref. 20. The transmission matrix of the nozzle is the product of the transmission martices for each segment. This procedure is used in Ref. 2 for the case of zero convected entropy. It is experimentally verified for the case of sound propagation in a variable area duct without flow in Ref. 21.

In order to calculate the nozzle pressure transfer function, two boundary conditions are needed. For one boundary condition, it is assumed that the

nozzle exit impedance is given by a model proposed by Lumsdaine and Ragab (Ref. 22). The second boundary condition is the ratio of the convected entropy perturbation to the acoustic pressure at the nozzle exit as a function of frequency and it is determined empirically.

THEORY

The following assumptions are made to obtain the plane wave acoustic equations: the duct has an area profile $A(x)$; the acoustics are described by first order, linearized equations of continuity, momentum, energy and state for isentropic sound propagation.

State variable equation

The one dimensional flow in the nozzle of a nonviscous, nonconducting, perfect gas is described by the familiar equations of continuity, momentum, energy and state (Eqs. (1) to (4) of Ref. 2).

The fluctuations in the duct are assumed so small that the flow in the duct is only slighthly perturbed. Consequently, the instantaneous quantities can be written in terms of a unperturbed stationary flow quantity designated by 0 and a small perturbed quantity designated by 1 (Eqs. (5) to (8) in Ref. 2).

Substituting the equations for the instantaneous quantities into the equations of continuity, momentum, and energy yields at zeroth order one system of equations (Eqs. (9) to (11) of Ref. 2) and at first order another system of equations (Eqs. (12) to (14) of Ref. 2).

For the system under consideration the gas is assumed to be a perfect gas.

The undisturbed flow is assumed to be steady and isentropic so that s_o and (p/ρ_o^γ) are constant in time. Consequently, the energy perturbation equation (Eq. (14) of Ref. 2) can be integrated to

$$\sigma(t,x) = s_1(t,x)/c_v = \frac{p_1(t,x)}{p_o(x)} - \frac{\gamma\,\rho_1(t,x)}{\rho_o(x)}$$

$$= \sigma_e\left[t - \int_{x_e}^{x} \frac{dx}{u_o(x)}\right] \tag{1}$$

Thus an entropy fluctuation is convected with the gas flow and its value remains unchanged from a value $\sigma_e(t)$ determined at the nozzle entrance, x = 0.0 .

In Ref. 2 the entrance entropy fluctuation was assumed to be negligible. Consequently, the density perturbaton was related to a pressure perturbation by

$$\rho_1 = p_1/c_o^2 \tag{2}$$

However, in this paper, the entrance entropy fluctuation is assumed significant and

$$\rho_1 = \frac{p_1}{c_o^2} - \frac{p_o}{c_o^2}\frac{s_1}{c_v} \tag{3}$$

The perturbed state variables are the acoustic pressure, the particle velocity, and the entropy. These quantities are assumed to vary with time as $\exp(-i\omega t)$. Substituting Eq. (3) into the Fourier transform of Eqs. (12) to (14) of Ref. 2 yields the following equation in matrix form:

$$\begin{bmatrix} u_o/\rho_o c_o^2 & 1 & -u_o/c_p \\ 1/\rho_o & u_o & 0 \\ 0 & 0 & u_o \end{bmatrix} \begin{pmatrix} dp_1/dx \\ du_1/dx \\ ds_1/dx \end{pmatrix}$$

$$+ \begin{bmatrix} \left\{\frac{(-i\omega)}{\rho_o c_o^2} + \left[\frac{u_o}{\rho_o c_o^2}\right]\left[\frac{d\ \ln(A)}{dx} + \frac{d\ \ln(u_o)}{dx}\right]\right\} & \left\{\frac{d\ \ln A}{dx} + \frac{d\ \ln(\rho_o)}{dx}\right\} & \left\{-\frac{(-i\omega)}{c_p} - \frac{u_o}{c_p}\left[\frac{d\ \ln(A)}{dx} + \frac{d\ \ln(u_o)}{dx}\right]\right\} \\ \left[\frac{u_o^2}{\rho_o c_o^2}\right]\frac{d\ \ln(u_o)}{dx} & \left\{(-i\omega) + u_o\frac{d\ \ln(u_o)}{dx}\right\} & -\frac{u_o^2}{c_p}\frac{d\ \ln(u_o)}{dx} \\ 0 & 0 & (-i\omega) \end{bmatrix} \begin{pmatrix} p_1 \\ u_1 \\ s_1 \end{pmatrix} = 0 \tag{4}$$

The differential equations used in Refs. 4 and 5 to model a variable area duct with acoustic and convected entropy perturbations differ from the familiar first-order acoustic equations in two respects. They have additional terms on the left hand side which represent the changes in the field due to gradients in the duct geometry, mean flow and density. Furthermore, they have dipole source terms on the right hand side which arise from the interaction of

the entropy fluctuation with gradients of the duct geometry and mean flow. Consequently, in these analytical models the entropy fluctuation is viewed as a source term and the equations are treated as being nonhomogenous. Thus, in order to solve these equations an acoustic impedance must be specified at the start and end of the source regic·: and the entropy fluctuation must be specified at a point in the region.

However, in this paper the first-order equations are written with the terms which arise from the interaction of the entropy fluctuation with the gradients of the duct geometry and mean flow on the left hand side. As a result the equations have no source terms. Thus only propagation occurs and the equations are homogeneous. Thus, in order to solve these equations only two boundary conditions at an end of the propagaton region are necessary. As a result, specifying an acoustic impedance boundary condition and the ratio of the convected entropy perturbation to the acoustic pressure as a function of frequency at the same end of the propagation region is sufficient to generate a solution.

The gradients of the logarithmical variation of velocity and density are related to the logarithmical variation of area as follows:

$$\frac{d\ \ln(u_o)}{dx} = -\frac{1}{1 - M_o^2}\frac{d\ \ln(A)}{dx} \tag{5}$$

$$\frac{d\ \ln(p_o)}{dx} = \frac{M_o^2}{1 - M_o^2}\frac{d\ \ln(A)}{dx} \tag{6}$$

Substituting Eqs. (5) and (6) into Eq. (4) and solving for dY/dx where Y = (p_1, u_1, s_1) yields

$$dY/dx = BY \tag{7}$$

where the elements of the B matrix are:

$$B_{11} = \frac{M_o\,(-ik_o)}{1 - M_o^2} + \frac{M_o^2}{1 - M_o^2}\,\frac{d\,\ln(A)}{dx} \tag{8}$$

$$B_{12} = \frac{\rho_o c_o (ik_o)}{1 - M_o^2} + \frac{\rho_o c_o\, 2\, M_o}{(1-M_o^2)^2}\,\frac{d\,\ln(A)}{dx} \tag{9}$$

$$B_{13} = -\,\frac{\rho_o c_o^2}{c_p}\,\frac{M_o^2}{1 - M_o^2}\,\frac{d\,\ln(A)}{dx} \tag{10}$$

$$B_{21} = \frac{ik_o}{\rho_o c_o\,(1 - M_o^2)} \tag{11}$$

$$B_{22} = \frac{M_o\,(-ik_o)}{1 - M_o^2} - \frac{(1+M_o^2)}{(1-M_o^2)^2}\,\frac{d\,\ln(A)}{dx} \tag{12}$$

$$B_{23} = 0 \tag{13}$$

$$B_{31} = 0 \tag{14}$$

$$B_{32} = 0 \tag{15}$$

$$B_{33} = i\omega/u_o \tag{16}$$

where $k_0 = \omega/c_0$. Note that the 3x3 B matrix in Eq. 7 differs from the 2x2 acoustic propagation B matrix discussed in Ref. 2 by the addition of matrix element B_{13} which gives the change in the gradient of the acoustic pressure due to the convected entropy and matrix element B_{33} which gives the change in the entropy gradient due to the convected entropy. The acoustic-convected entropy state variable differential equation is given by Eq. (7). This equation will be solved next.

Method of solution

In the previous section a general acoustic-convected entropy state variable differential equation was derived (Eq. (7)). In this section an approximate solution is found. A method of solution similar to the one used in this study is presented in Ref. 2. However, in Ref. 2 it is applied only to the acoustic equations. For clarity, it is briefly discussed and those modifications nedessary to adopt it to these acoustic-convected entropy equations are given. The first step in obtaining a solution to Eq. (7) is to divide the duct into a number of regions or subsections. The region size is selected so that the area variation in each region can be approximated by an exponential area variation. Consequently, in a given region

$$M_0 = \text{constant} \tag{17}$$

and

$$A = A_0 e^{mx} \tag{18}$$

With this assumption the value of $d \ln(A)/dx$ is a constant in the region given by

$$m = d \ln(A)/dx \tag{19}$$

The B matrix in Eq. (7) is now independent of x in the region where it is to be evaluated. Thus, the solution to Eq. (7) for the jth region is

$$Y(x_j + \Delta x) = (e^{B \Delta x})_j \, Y(x_j) \tag{20}$$

where x is the length of the jth region and $\exp(B \Delta x)$ is known as the matrix exponential. The matrix $\exp(B \Delta x)$ is the transmission matrix of the jth region, $(T)_j$, so that

$$(T)_j = (e^{B \Delta x})_j = \sum_{\ell=0}^{\infty} \frac{(B \Delta x)_j^{\ell}}{\ell!} = \begin{bmatrix} T_{11} & T_{12} & T_{13} \\ T_{21} & T_{22} & T_{23} \\ 0 & 0 & T_{33} \end{bmatrix} \tag{21}$$

Consequently, the transmission matrix T for the variable area duct is found from

$$Y(x=L) = \prod_{j=1}^{N} (e^{B \Delta x})_j \, Y(x=0) = TY(x=0) \tag{22}$$

where

$$L = \sum_{j=1}^{N} (\Delta x)_j \tag{23}$$

and N is the number of nozzle regions.

Evaluation of matrix exponential

While the series given in Eq. (21) defines the matrix exponential, it was not used for computer calculations since the convergence of the series may be slow. The matrix exponential was evaluated from

$$e^{B\,\Delta x} = C^{-1}\, P e^{D\,\Delta x}\, P^{-1}\, C \tag{24}$$

where

$$D = P^{-1}\, \mathcal{A}\, P \tag{25}$$

$$\mathcal{A} = CBC^{-1} \tag{26}$$

$$C = \begin{bmatrix} 1 & 0 & 0 \\ 0 & \rho_o c_o & 0 \\ 0 & 0 & \rho_o c_o^2/c_p \end{bmatrix} \tag{27}$$

and P is determined below such that the matrix D is diagonal. The P matrix then consists of eigenvectors of $\mathcal{A}$.

The matrices in Eq. (24) as used in Ref. 2 are 2x2 since acoustic pressure and particle velocity are the only variables. However, as used herein the matrices are 3X3 since entropy perturbations are being included. Consequently, the C matrix contains a new element. Furthermore, the eigenfunction P matrix used herein has a new definition dependent on the eigenvalues λ_1, λ_2, and λ_3 of the $\mathcal{A}$ matrix.

For $j = 1$ and 2 the column eigenvector of P is selected as follows:

$$P_{j1} = (\mathcal{A}_{22}-\lambda_j)\ (\mathcal{A}_{33}-\lambda_j) \tag{28}$$

$$P_{j2} = -\ \mathcal{A}_{21}\ (\mathcal{A}_{33}-\lambda_j) \tag{29}$$

$$P_{j3} = 0 \tag{30}$$

However, the third column of P is selected to be

$$P_{31} = -\ \mathcal{A}_{13}\ (\mathcal{A}_{22}-\lambda_3) \tag{31}$$

$$P_{32} = \mathcal{A}_{21}\ \mathcal{A}_{13} \tag{32}$$

$$P_{33} = (\mathcal{A}_{11}-\lambda_3)\ (\mathcal{A}_{22}-\lambda_3) - \mathcal{A}_{12}\ \mathcal{A}_{21} \tag{33}$$

The values of λ_1, λ_2, and λ_3 are the eigenvalues of the matrix. The values of λ_1 and λ_2 are given by the roots of

$$\lambda^2 + b\lambda + c = o \tag{34}$$

where

$$b = -\ (\mathcal{A}_{11}+\mathcal{A}_{22}) \tag{35}$$

and

$$c = \mathcal{A}_{11}\ \mathcal{A}_{22} - \mathcal{A}_{12}\ \mathcal{A}_{21} \tag{36}$$

The value of λ_3 is given by

$$\lambda_3 = i\omega/u_o \tag{37}$$

It can be verified that

$$D = \begin{pmatrix} \lambda_1 & 0 & 0 \\ 0 & 0 & 0 \\ 0 & 0 & \lambda_3 \end{pmatrix} \tag{38}$$

hence

$$e^{D\,\Delta X} = \begin{pmatrix} e^{\lambda_1 \Delta X} & 0 & 0 \\ 0 & e^{\lambda_2 \Delta X} & 0 \\ 0 & 0 & e^{\lambda_3 \Delta X} \end{pmatrix} \tag{39}$$

Nozzle exit acoustic boundary conditions

The nozzle calculations shown herein are made using the following duct exit impedance

$$\frac{Z}{\rho_o c_o} = M_o + \quad 1 - 2\, J_1(\nu)/\nu \quad - i\ \mathcal{S}_1(\nu)/\nu \tag{40}$$

where

$$\nu = 2\, k_o r_d \Big/ (1-M_o^2)^{1/2} \tag{41}$$

$J_1(\nu)$ is the Bessel function of the first order and first kind, $\mathcal{S}_1(\nu)$ is the Struve function of the first kind and first order, and r_d is the nozzle exit radius. The duct exit impedance was derived in Ref. 22 for a circular duct with flow having an open end fitted with an infinite acoustically rigid flang. Note that in the case of outflow, M is replaced by $-M$ in Eq. (40).

Calculation of nozzle transfer function

The transfer function between point (2) near the core nozzle entrance and point (1) near the core nozzle exit is calculated using the acoustic pressure at the core nozzle entrance, p_s (x=0.0), the acoustic impedance at the core nozzle entrance, Z(x=0.0), and the convected entropy at the core nozzle, Σ_s (x=0.0), as follows:

$$p\ (2) = \left[T_{11}\ (2) + \frac{T_{12}\ (2)}{Z\ (x=0.0)} \right] p_s\ (x=0.0) + T_{13}\ (2)\ \Sigma_s(x=0.0) \tag{42}$$

and

$$p\ (1) = \left[T_{11}\ (1) + \frac{T_{12}\ (2)}{Z\ (x=0.0)} \right] p_s\ (x=0.0) + T_{13}\ (1)\ \Sigma_s(x=0.0) \tag{43}$$

The transfer function, H(f), is the ratio of p(1) to p(2)

$$H\ (f) = p\ (1)/p\ (2) \tag{44}$$

Consequently, the major effect of convected entropy depends on the transfer function relating entropy and pressure at the nozzle inlet.

However, the acoustic impedance at the core nozzle entrance is also a function of the entropy. The acoustic impedance at the exit is assumed to be independent of the convected entropy. The acoustic impedance at the core nozzle entrance Z(x=L) is found from the acoustic impedance at the core nozzle exit, the convected entropy at the inlet and the convection time delay using the following relationship:

$$\begin{pmatrix} p\ (x=0) \\ p\ (x=0)/Z\ (x=0) \\ \\ \Sigma\ (x=0) \end{pmatrix} = T^{-1} \begin{pmatrix} 1 \\ 1/Z\ (x=L) \\ \\ \Sigma\ (x=0)\ e^{-i\omega \int_0^L dx/u_o\ (x)} \end{pmatrix} \tag{45}$$

The absolute value of p_s (x=0.0) does not determine the nozzle transfer function. The value of the convected entropy and the convected entropy-pressure transfer function at the entrance determine the nozzle transfer function. The value of p_s (x=0.0) is selected so that for zero convected entropy the calculated value of the auto pressure spectra at points one and two are similar the the measured pressure auto-spectra at these points. Since the measured pressure auto-spectra may be due to both acoustic and nonacoustic pressure perturbations they were not used directly.

In order to define an acoustic pressure at the core nozzle inlet to use as p_s, a fictitious point pressure source was placed at the core nozzle entrance. This point pressure source was assumed to have a $(f)^{-1}$ spectrum. The spectrum level was determined by single constant selected to make the calculated and measured auto spectra appear similar. A Green's function solution was then constructed in a small region about this hypothetical point source using the source region model described in Ref. 23. The upstream impedance was constructed by assuming the reflection factor was 0.9. The downstream impedance was the core nozzle inlet impedance, Z(x=0.0).

In these calculations the pressure at the entrance is real. However, the phase relationship of the pressure and entropy perturbations is not known. Consequently, two arbitrary phase relationships of pressure and entropy were used in the computational study. Most calculations were made using

$$\Sigma_s\ (x=0) = |\Sigma_s|\ e^{i\omega \int_0^L dx/u_o\ (x)} \tag{46}$$

so that the convected entropy and pressure were in phase at the core nozzle exit. While this relations is unrealistic, it has the advantage that changes in the transfer function with changes in the magnitude of Σ_s could be more easily compared to the case where Σ_s is zero. In order to obtain some information on the importance of the phase relationship between pressure and flow, some calculations were made using

$$\Sigma_s\ (x=0) = |\Sigma_s| \tag{47}$$

For this case the convected entropy is real at the entrance and out of phase with the pressure at the exit by $\omega \int_0^L dx/u_o\ (x)$.

Various values of the magnitude of the convected entropy were used. For the cases presented the magnitude of Σ_s was selected to be large enough to show the effects of its presence.

EXPERIMENTAL DATA

The Pratt & Whitney JT15D is a bypass ratio 3.3, two-spool, turbofan engine with a rated thrust for 9800 Newtons. The engine core consists of a compressor in the form of a 16-bladed impeller, a reverse flow annular combustor, and a three-stage turbine. The single-stage compressor is driven by the high-pressure turbine stage, while the fan is driven directly by the two low-pressure turbine stages. The fan has twenty-eight blades and is 0.534 m in diameter.

The test data are discussed in Ref.1. All tests were conducted using an outdoor engine test stand. The engine was mounted with the engine centerline 2.9 m above a hard surface ground plane. The engine was fitted with an inlet control device to reduce fan tones by providing a cleaner and more uniform inflow than is normally obtained under static test conditions. A photograph of the engine mounted on the test stand is shown in Fig. 1.

Dynamic pressure probes were placed in the engine core at seven different locations (Fig. 2). Data used herein were measured using probes at the core nozzle entrance and at the core nozzle exit plane. The core nozzle geometry and microphone locations are shown in Fig. 3. The transducers used were conventional 0.635 cm diameter pressure response condenser microphones. To avoid direct exposure of the microphone to the severe environment within the core, they were mounted outside the engine and the fluctuating pressure in the engine core was communicated to the transucers by "semi-infinite" acoustic waveguides. These wavequide probes are described in detail in Ref. 24. Data were also taken using far-field microphones. Data acquisition and processing are described in more detail in Ref. 1. Test conditions for the noise measurements used herein are given in Table I.

In order to calculate a noise-free acoustic transfer function, the experimental transfer function is calculated from

$$H = \frac{p(1)}{p(2)} = \frac{p(1)\ p^*(e)}{p(2)\ p^*(e)} \tag{48}$$

where $p(2)p^*(e)$ is the cross-spectrum between the microphone at the nozzle inlet and a far-field microphone and $p(1)p^*(e)$ is the cross-spectrum between the turbine exit microphone and a far-field microphone.

RESULTS

Transmission matrix

Transmission matrices for the duct configuration shown in Fig. 3 with and without flow were numerically calculated using Eq. 40. The calculations yield an exact solution for the case where the Mach number is zero and an approximate solution for the case with flow. The approximation is improved as the core nozzle is divided into smaller subsections. The matrices were calculated using 230 equal length subsections. Typical elements of the transmission matrices T calculated with and without flow are shown in Fig. 4 where

$$Y\ (x=39.5\ \text{cm}) = T\ y\ (x=0.0) \tag{49}$$

For the solution with flow, the zeroth-order system of equations is solved to evaluate p, u , ρ, and θ at the start of each subsection using a stagnation pressure of 1.0076 atmosphere, a stagnation temperature of 414 C and a mass flow rate of 2.73 kg/s.

The acoustic matrix elements, T_{11}, T_{12}, T_{21}, and T_{22} for the cases with and without flow are similar to the corresponding transmission matrix elements of the long exponential nozzle shown in Fig. 2 of Ref. 2. The convected entropy matrix elements T_{13}, T_{23} and T_{33} are new results. Matrix element T_{33} yields no new information for it merely shows that the entropy is convected unchanged. However, matrix element T_{13} shows the amount the core nozzle exit pressure is changed by an inlet entropy perturbation and matrix element T_{23} shows the amount the core nozzle exit acoustic particle velocity is changed by an inlet entropy perturbation if the inlet acoustic pressure and particle velocity are zero. Note that the phase of the matrix elements T_{13} and T_{23} is strongly dependent on the convection velocity.

Transfer function calculations

The entropy spectrum Σ_s is related to the gas temperature spectral density since

$$\frac{|\Sigma_s|}{c_p} = \frac{\theta}{\theta_0} - \frac{p}{p_0}\frac{(1-\gamma)}{\gamma} \cong \frac{\theta}{\theta_0} \tag{50}$$

where the pressure term is neglected since the acoustic pressure perturbation is much smaller than the mean pressure. However, no measurements of the gas temperature spectrum in the nozzle were available. The existence of a gas temperature spectrum in the nozzle can be inferred from the rms and power spectral density gas temperature measurements in a gas turbine transition duct exit presented in Ref. 25.

Since no spectral data were available, the acoustic pressure transfer function was calculated to show the effect of a particularly large rms temperature standard deviation in a single 1 Hz frequency band. The standard deviation over a frequency range f_0 is related to the temperatue power spectral density by

$$\sigma_\theta^2 = \int_0^{fo} S_\theta \, d\, f \tag{51}$$

Consequently, the power spectral density S_θ is much lower than θ^2/Hz if the standard deviation in the frequency band is 0.

Most calculations were made using $|\Sigma| = 50.0$ J/kg K. At the lowest test condition when the nominal engine speed is 33 percent of the maximum, $c_p = 1083$ J/kg K, and $\theta_0 = 675$ K. Consequently, the corresponding rms temperature deviation is about 31 K. This corresponds to having an rms deviation of 31 K where the temperature is excited over a narrow 1-Hz band-

width. If the temperature spectrum was band-limited with noise up to 1200 Hz, the rms deviation of 31 K over this frequency range would imply that the convected entropy magnitude was 1.44 J/kg K.

Comparison with experimental data

Transfer functions were calculated using various models and compared with experimental data. Some typical results are presented next. Figure 5 show that the transfer function measured at a nominal engine speed of 33 percent of the maximum engine speed. Also shown in Fig. 5 are transfer functions calculated for the following cases: (1) no flow, (2) with flow but with no convected entropy, and (3) with flow and convected entropy with $|\Sigma_s|$ = 50.0 J/kg K and the convected entropy and pressure in phase at the nozzle exit.

The measured transfer function magnitude and phase plots contain much scatter. Due to the scatter in the magnitude plot shown in Fig. 5(a), all the methods for calculating the transfer function magnitude appear to agree with the data over the frequency range from 120 Hz to 720 Hz. Furthermore, all three methods fail to yield the correct magnitude above 720 Hz where higher mode propagation may be important. Also, only the zero flow case fits the magnitude data below 120 Hz.

The measured transfer function phase angle plots shown in Fig. 5(b) have less scatter below 720 Hz. Comparing the calculated and measured transfer function phase angle curves shows that most of the data are bounded between the phase angle curve calculated for the flow and no-flow cases for the frequency range from 120 Hz to 720 Hz. However, the calculations made for the cases with flow are in better agreement. Nevertheless, of the two cases with flow, only small differences occur beteeen the cases with and without convected entropy.

The one-dimensional acoustic propagation theory for a variable area duct with flow applied using the duct exit impedance model of Lumsdaine and Ragab (Ref. 22) in general produced good agreement with the data. However, the results are not precise enough to indicate the presence or absence of convected entropy effects. The one-dimensional acoustic propagation theory for a variable area duct without flow has been verified experimentally (Ref. 21) and it is assumed to be valid with flow. However, the duct exit impedance used is only approximate since it was derived for a circular duct with flow having an open end fitted with an infinite acoustically-rigid flange. Consequently, an improved model for the nozzle exit impedance based on the geometry and flow at the JT15D turbofan engine core nozzle is needed in order to study the convected entropy effect.

Figure 6 shows the measured auto-spectra near the inlet and exit of the core nozzle at the nominal engine speed of 33 of the maximum engine speed. Also shown in Figure 6 are calculated auto-spectra for the same examples used in Fig. 5. Note that the measured and calculated core nozzle inlet auto-spectra have a dip near 500 Hz and a peak near 800 Hz. The calculated pressure auto-spectra level was adjusted to peak near 135 dB at 850 Hz.

Figure 7 compares the transfer function measured at 33 percent of the maximum engine speed with the transfer function calculated with $|\Sigma_s| = 50.0$ and 100.0 J/kg K and the convected entropy and pressure in phase at the nozzle exit. Increasing the level of the convected entropy does not produce better agreement.

The transfer function curves shown in Figs. 5 and 7 were calculated with the convected entropy and pressure in phase at the exit. These transfer function curves are smooth. In Fig. 8 the transfer function calculated using Eq. 47 with the convected entropy and pressure out of phase at the exit are

shown. This transfer function is calculated for the case where the convected entropy has a zero phase angle at the entrance. The resulting transfer function amplitude and phase angle curves have dips and peaks. Consequently, the phase relationship between the convected entropy and pressure must be measured in order to know if the dips and peaks in the transfer function phase angle data can be attributed to convected entropy.

For the given geometry and the measured auto spectra the value of the convected entropy had to be 50/kg K in order to see a significant convected entropy effect. This value might occur in a single frequency 1 Hz band because it represents a standard deviation of 31 K in a 1 Hz band. However, it cannot exist over a large frequency range or the standard deviation would be larger than the average. Consequently, it is more likely that the value of the convected entropy is of the order 1.44 J/kg K over the frequency range from 0 to 1200 Hz so that the standard deviation is 31 K in the band from 0 to 1200 Hz. However, if the convected entropy is of this order then no effect would be observed. Furthermore, this is true independent of the phase of the convected entropy. Thus, the effect of convected entropy on the nozzle transfer function at this test condition is so negligible at most frequencies that it is obscured by the scatter in the data and use of an incorrect nozzle exit impedance.

These results show that the calculated transfer function with flow and with and without convected entropy resembles the data measured at 33 percent of the maximum engine speed. Moreover, they indicate that convected entropy could be a factor in defining the transfer function. Furthermore, these results indicate that the phase relationship of the convected entropy to the pressure is as important as magnitude information.

Calculations were also made to determine if the model transfer function resembled the data measured at other engine speeds. In Fig. 9 is shown the measured transfer function magnitude and phase angle plots at 33 percent, 40 percent, 55 percent, 87 percent, and 97 percent of the maximum engine speed. Also shown in Fig. 9 is the transfer function calculated without and with flow, using $|\Sigma_s| = 50$ J/kg K, and using the convected entropy and pressure in phase at the core nozzle exit. Examination of the calculations at 33 percent of the maximum engine speed shown in Fig. 5 indicates that the the transfer function calculated using this value of $|\Sigma_s|$ is essentially identical to that calculated for $|\Sigma_s|$ equal to zero. Thus, in Fig. 9, essentially transfer functions calculated with and without flow are compared at the lower engine speeds.

Examination of the measured transfer function magnitude curves shown in Fig. 9 indicates that while the nozzle exit Mach number varies from 0.16 to 0.56, the magnitude plots do not change significantly over the entire range. The measured phase angle curves do show some change with operating conditions. The phase angle curves measured for nominal engine speeds of 33 percent, 40 percent and 55 percent form a similar group. For example, the phase angle between 120 and 240 Hz is about 20 degrees for these low engine speeds. The phase angle curves measured at the higher speeds 87 percent and 97 percent form a different group. For this group, the phase angles are near 45 degrees over the frequency range from 120 to 240 Hz.

Comparing the transfer function magnitudes calculated with and without flow with the measured transfer functions at 33 percent and 40 percent engine speed shows good agreement with both theories. However, the transfer function calculated for the variable area nozzle with flow fits the phase angle best.

Surprisingly, the transfer function calculated without flow is in fair agreement with the measurements at all engine speeds. This shows that while the nozzle exit impedance model used is adequate at the low flow conditions, at the higher flow conditions a more adequate model for the exit impedance and more information about the convected entropy is needed.

CONCLUDING REMARKS

An acoustic transmission matrix analysis of sound propagation in a variable area duct with flow and convected entropy fluctuations was presented. The analysis was used with an acoustic impedance and an entropy-pressure transfer function exit boundary condition to calculate the acoustic-pressure transfer function between the inlet and the exit of a JT15D core turbofan engine nozzle. The one-dimensional model for sound propagation in a duct yields good results if the duct exit impedance model is adequate. In spite of the scatter in the data, it is possible to see that the impedance model used is adequate for low Mach number flows (M less than 0.2). and at frequencies from 120 to 720 Hz. It is believed that a more adequate duct exit impedance is required at higher Mach numbers and at frequencies less than 120 Hz.

In order to find the effect of the convected entropy, its magnitude and the transfer function between pressure and entropy must be known. However, for this set of data the effect of convected entropy seems so negligible that it is lost in the scatter of the phase angle data at the low engine speeds where the exit impedance model used works best. At the higher engine speeds, its existence is obscured by the failure of the exit impedance model. These results show that: (1) the one-dimensional sound propagation model does apply to the JT15D turbofan nozzle data; (2) in order to study the convected entropy

effect in a real engine it will be necessary to measure its magnitude and the entropy-pressure transfer function; and (3) the exit impedance model must be improved.

Acknowledgement

The author wishes to thank Eugene A. Krejsa for calculating the JT15D nozzle transfer function from the measured pressure signal and for many helpful discussions.

REFERENCES

1. M. Reshotko and A. Karchmer, NASA TM-81610, 1980.

2. J. H. Miles, J. Acoust. Soc. Am. 69(6), 1577 (1981).

3. J. E. Ffowcs Williams, in Annual Review of Fluid Mechanics, vol. 9, (Annual Reviews, Inc., Palo Alto, Calif., 1977), pp. 447-468.

4. S. M. Candel, Ph. D. thesis, California Institute of Technology, 1971.

5. F. E. Marble and S. M. Candel, J. Sound Vib. 55(2), 225 (1977).

6. M. S. Bohn, J. Sound Vib. 52(2), 283 (1977).

7. H. Y. Lu, AIAA paper 77-1366 presented at the AIAA 4th Aeroacoustics conference, Atlanta, Georgia, 1977.

8. J. E. Ffowcs Williams and M. S. Howe, J. Fluid Mech. 70(3), 605 (1975).

9. E. E. Zukoski and J. M. Auerbach, J. Eng. Power 98(1), 60 (1976).

10. J. M. Auerbach, Ph. D. Thesis, California Institute of Technology, 1975.

11. M. S. Bohn, Ph. D. Thesis, California Institute of Technology, 1976.

12. W. C. Strahle, M. Muthukrishnan, D. H. Neale and M. K. Ramachandra, NASA CR-135220, 1977.

13. M. Muthukrishnan, W. C. Strahle and D. H. Neale AIAA J. 16(4), 320 (1978).

14. G. G. Pickett, Presented at the Eighth International Congress on Acoustic, London, England, 1974 (unpublished).

15. N. A. Cumpsty and F. E. Marble, Proc. R. Soc. London Ser. A. 357, (1690) 323 (1977).

16. N. A. Cumpsty and F. E. Marble, J. Sound Vib. 54(2), 297 (1977).

17. H. S. Tsien, J. Am. Rocket Soc. 22(3), 139, 162 (1952).

18. L. Crocco and H. Cheng, Theory of combustion instability in liquid propellant rocket motors (Butterworths Scientific Publications, London, England, 1956), Appendix B pp. 168-187.

19. K. Ogata, State space analysis of control systems, (Prentice-Hall, Englewood Cliffs, N. J., 1967).

20. C. Moler and C. Van Loan, SIAM Rev. 20(4), 801 (1978).

21. J. H. Miles, NASA-TM 82741, 1981.

22. E. Lumsdaine and S. Ragab, J. Sound Vib 53(1), 47 (1977).

23. J. H. Miles and D. D. Raftopoulos, J. Acoust. Soc. Am. 68(6), 1711 (1980).

24. M. Reshotko, A. Karchmer, P. F. Penko, and J. G. McArdle, AIAA Paper 77-21 (1977); also J. Aircr. 14(7), 611 (1977).

25. R. R. Dils, J. Eng. Power 95(3), 265 (1973).

TABLE I. - TEST CONDITIONS FOR THE SELECTED JT15D

NOISE MEASUREMENT POINTS

Nominal engine speed, percent of maximum	Core mass flow, kg/s	Pressure, atm	Temperature, K	Exit speed of sound, m/s	Air speed, m/s		Mach number	
					exit	inlet	exit	inlet
33	2.3	0.997	675	515	81	40	0.16	0.08
40	2.7	1.008	687	519	96	47	.19	.09
55	3.8	1.037	717	529	136	67	.26	.13
87	6.6	1.097	772	543	198	94	.37	.17
97	7.8	1.264	878	569	320	142	.56	0.24

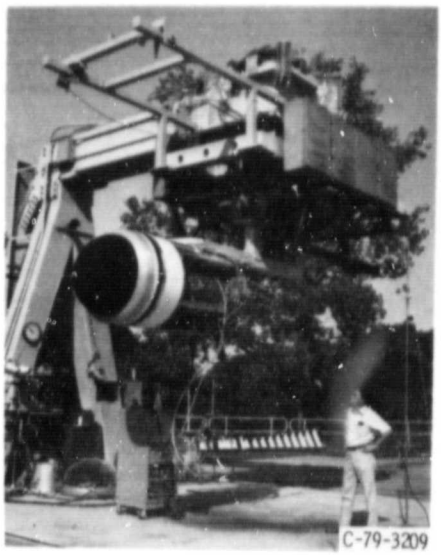

Figure 1. - JT15D turbofan engine on test stand.

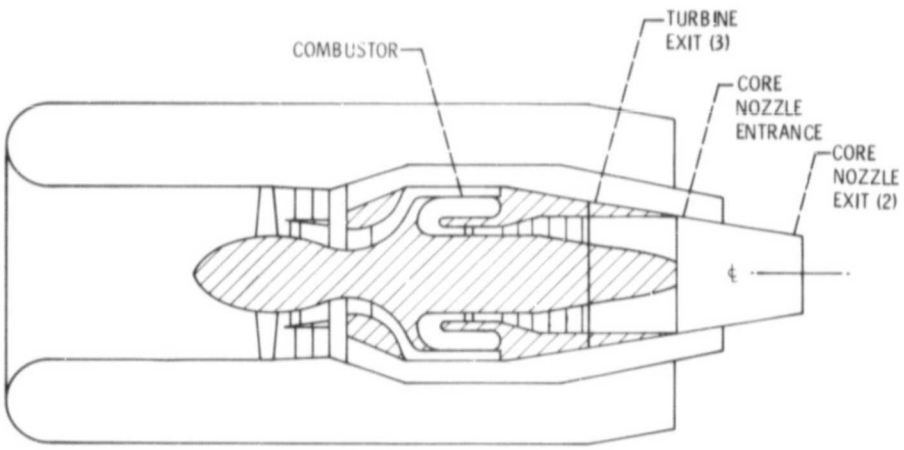

Figure 2. - Core acoustic waveguide probe locations.

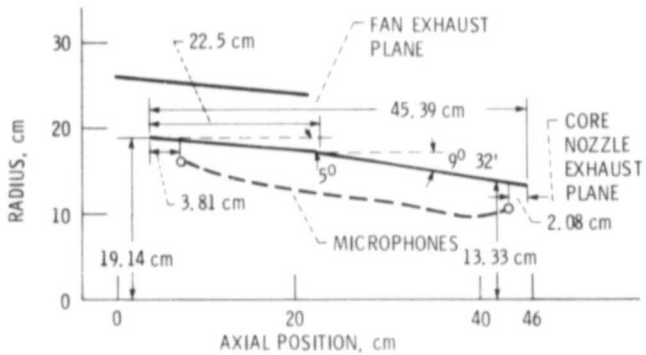

Figure 3. - Core nozzle geometry.

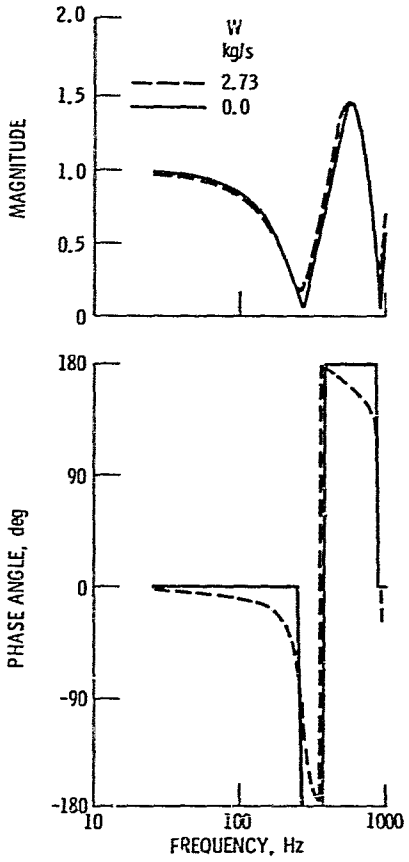

(a) T_{11}.

Figure 4. - JT15D core nozzle transmission matrix, T where Y(x=39.5cm) = T Y(x=0.0).

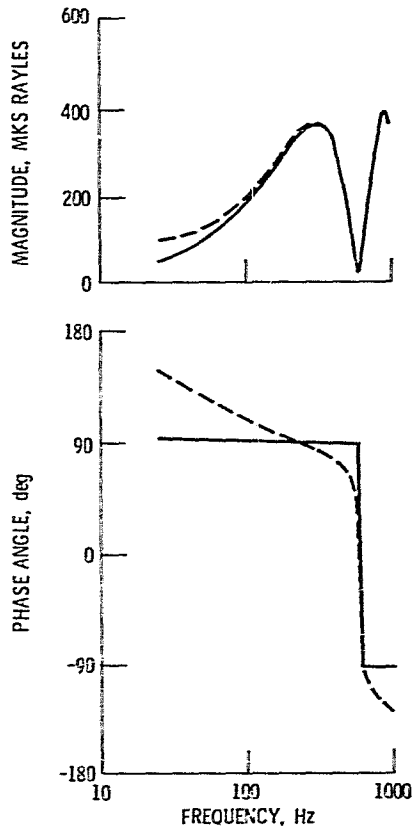

(b) T_{12}.

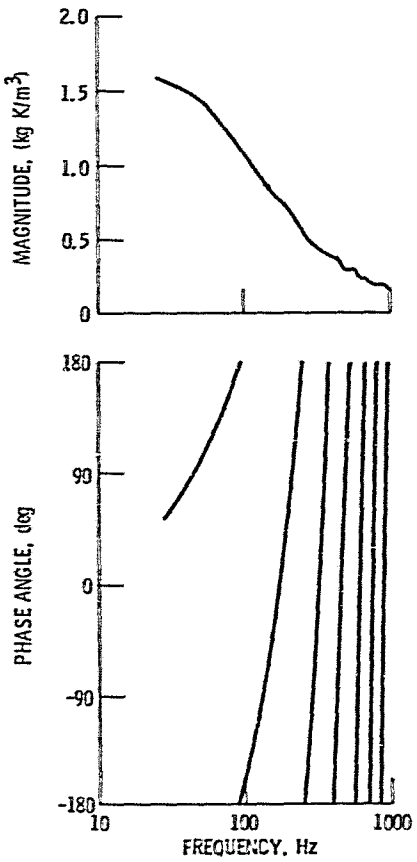

(c) T_{13}.

Figure 4. - Continued.

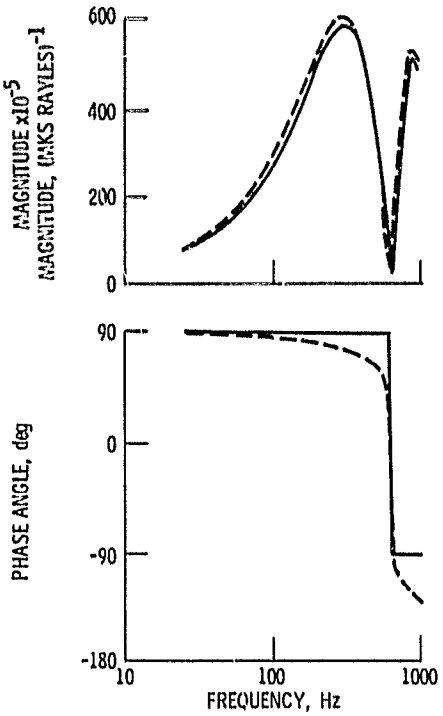

(d) T_{21}.

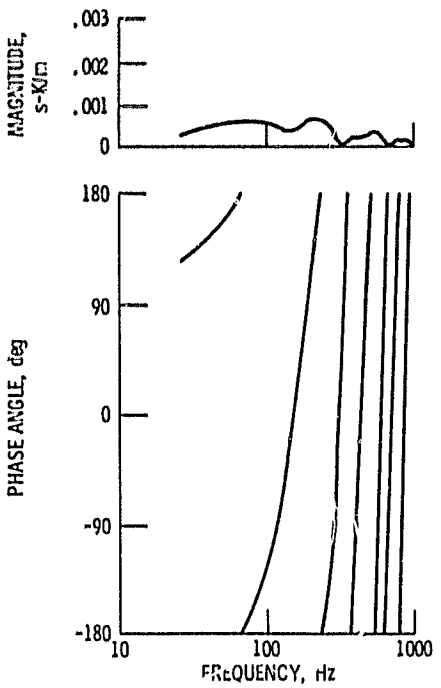

(f) T_{23}.

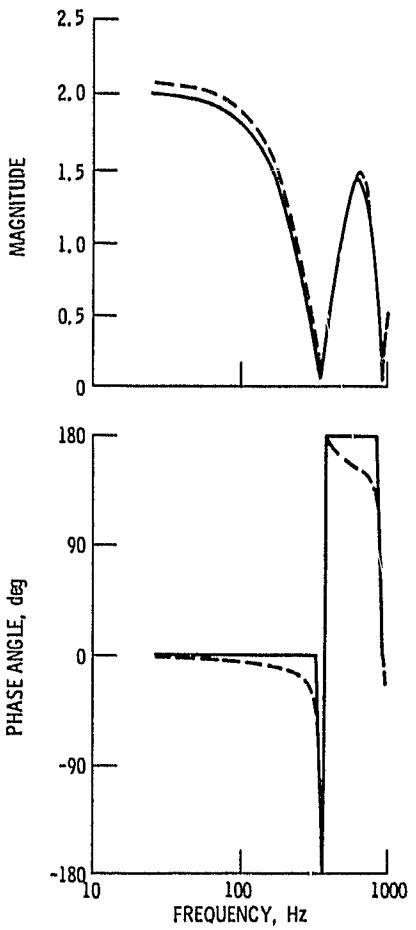

(e) T_{22}.

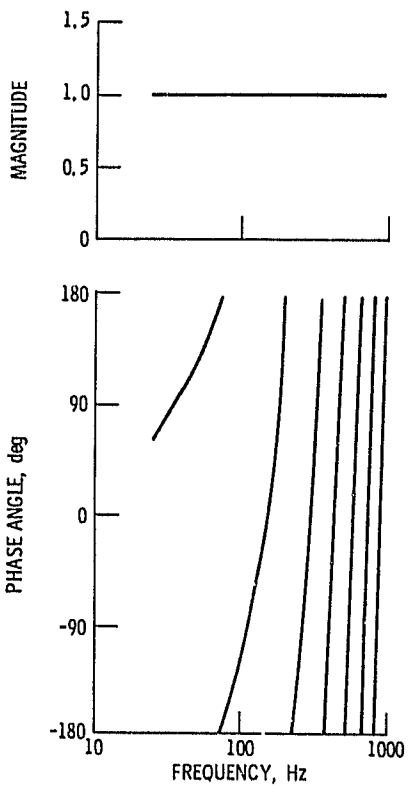

(g) T_{33}.

Figure 4. - Concluded.

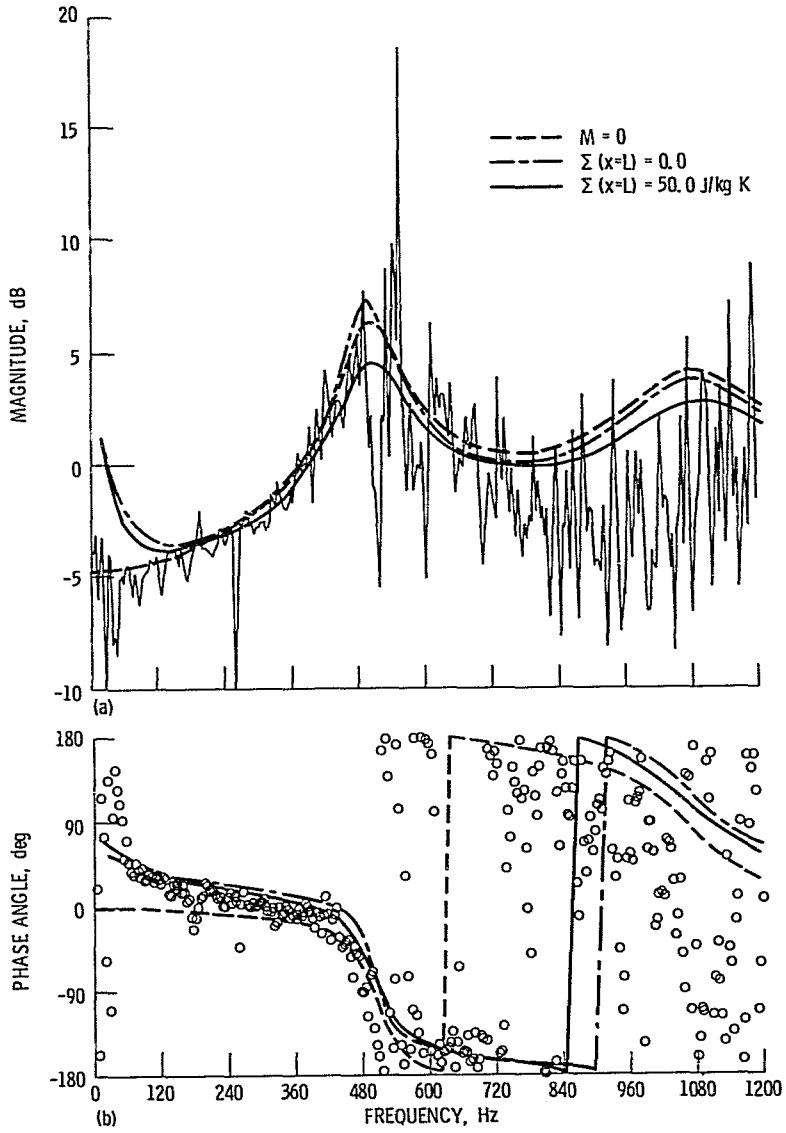

(a) Magnitude.

(b) Phase angle.

Figure 5. - Measured transfer function at 33% of maximum engine speed and calculated transfer functions.

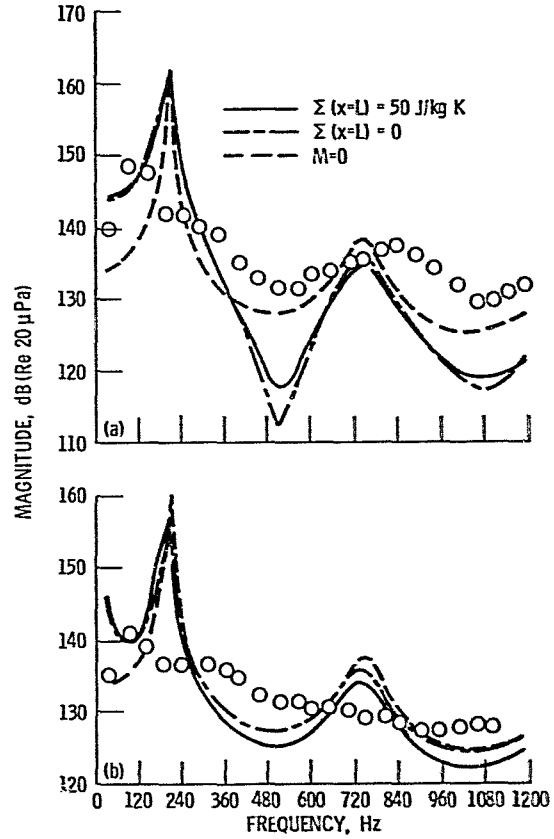

(a) Auto-spectra near core nozzle inlet.

(b) Auto-spectra near core nozzle exit.

Figure 6. - Measured auto-spectra at 33% of maximum engine speed and calculated auto-spectra.

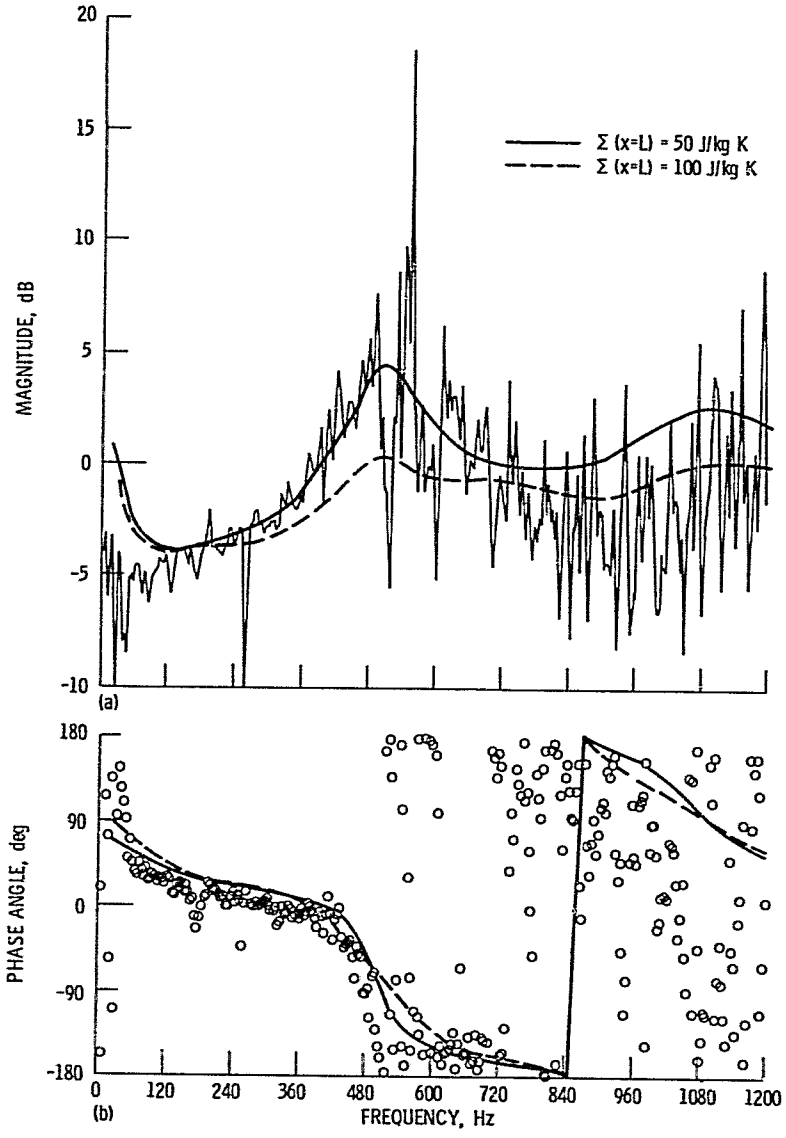

(a) Magnitude.

(b) Phase angle.

Figure 7. - Measured transfer function at 33% of maximum engine speed and calculated transfer functions for two values of Σ with Σ in phase with the pressure at the exit.

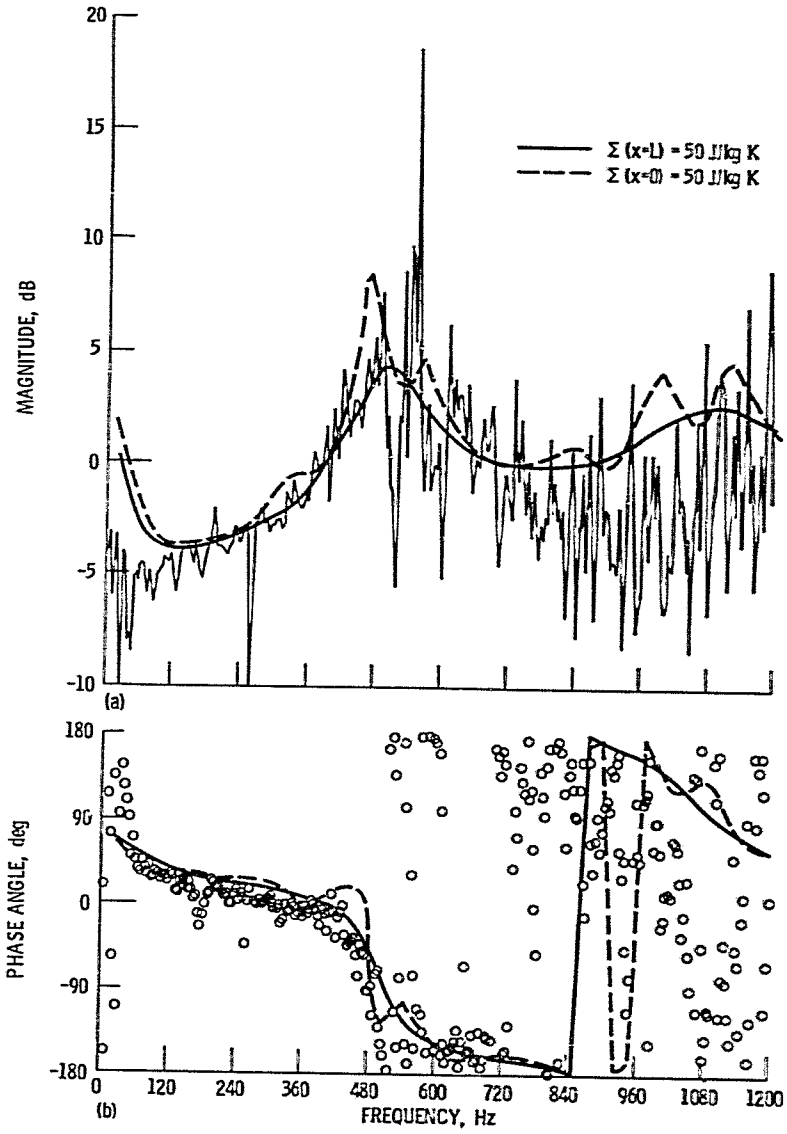

(a) Magnitude.

(b) Phase angle.

Figure 8. - Measured transfer function at 33% of maximum engine speed and calculated transfer functions using two different convected entropy phase relationships.

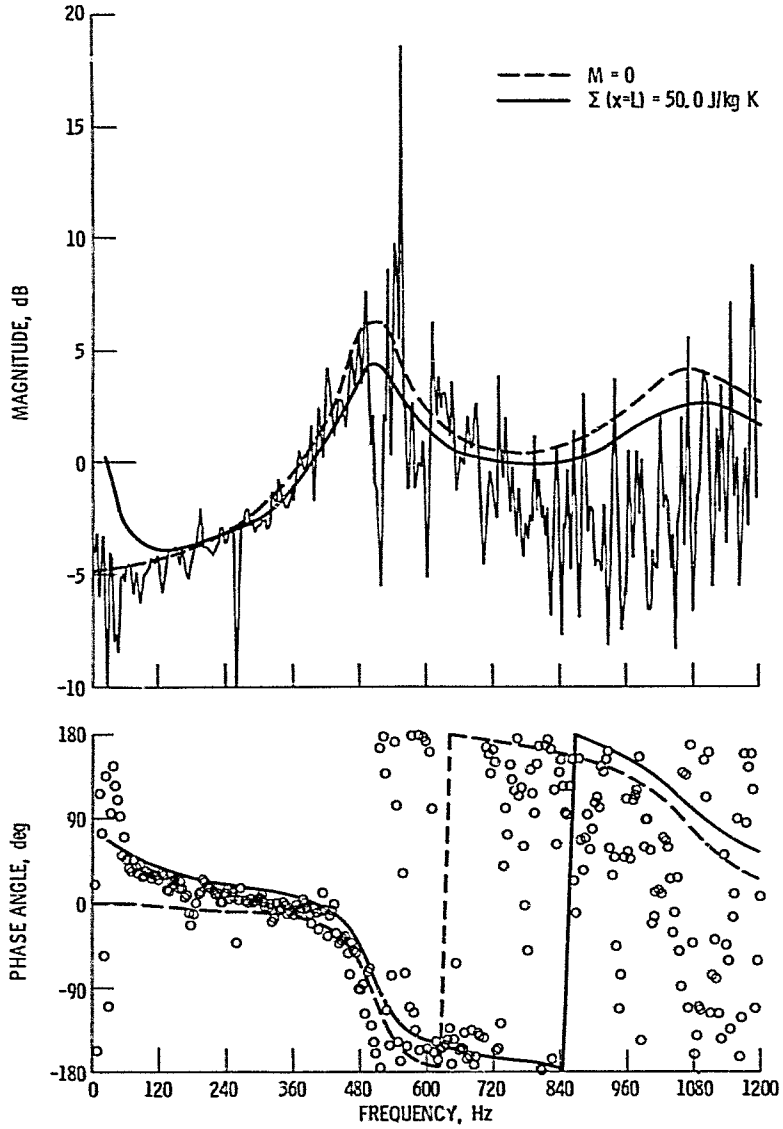

(a) JT15D nozzle transfer function 33%.

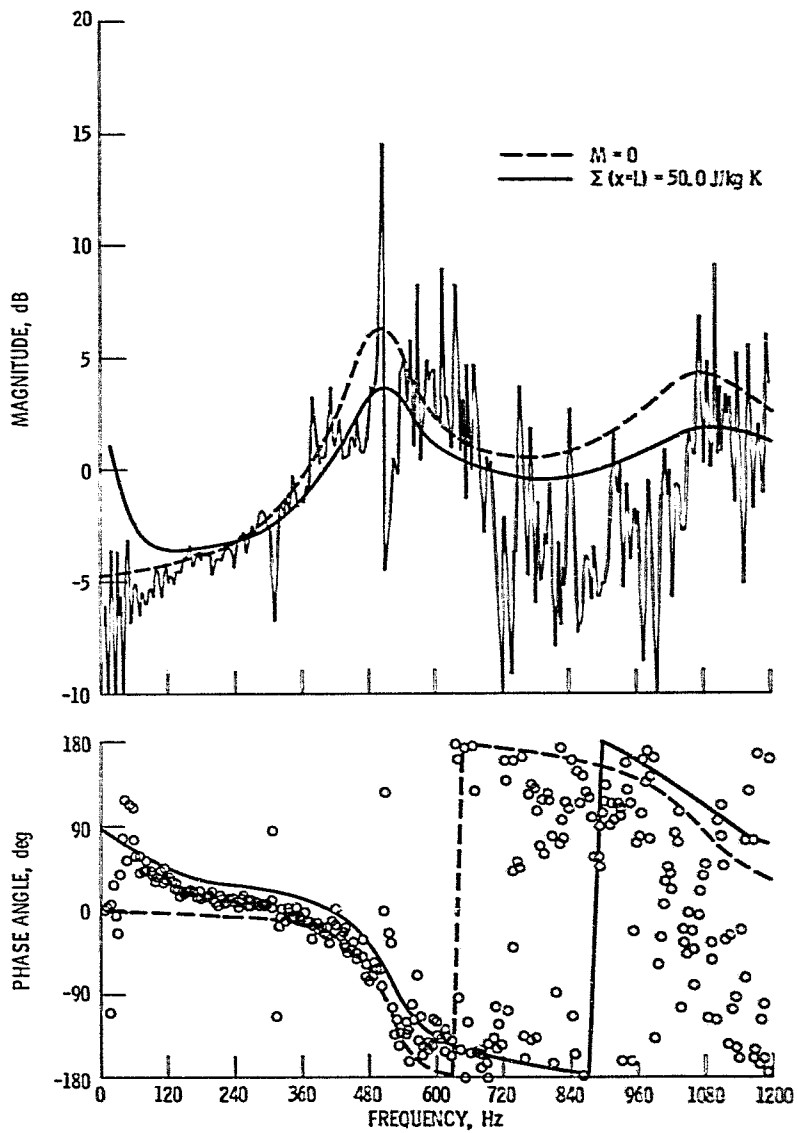

(b) JT15D nozzle transfer function 40%.

Figure 9. – Comparison of measured ar calculated transfer functions for a range of engine speeds.

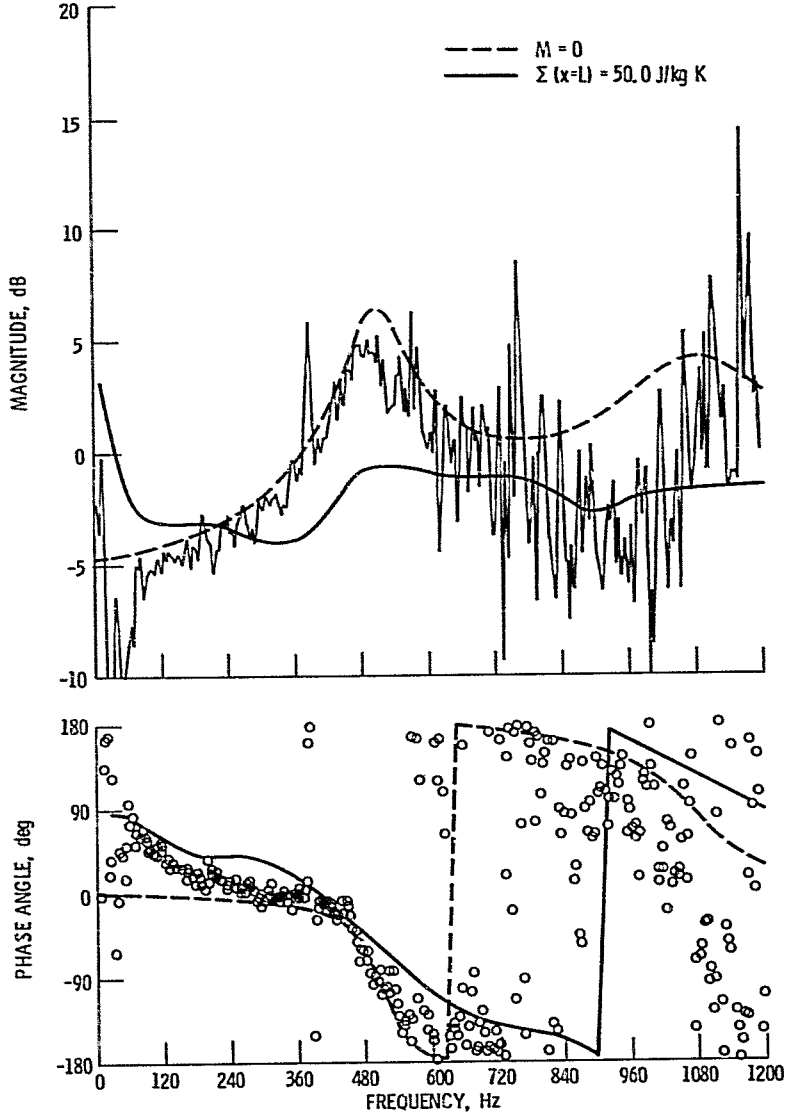

(c) JT15D nozzle transfer function 55%.

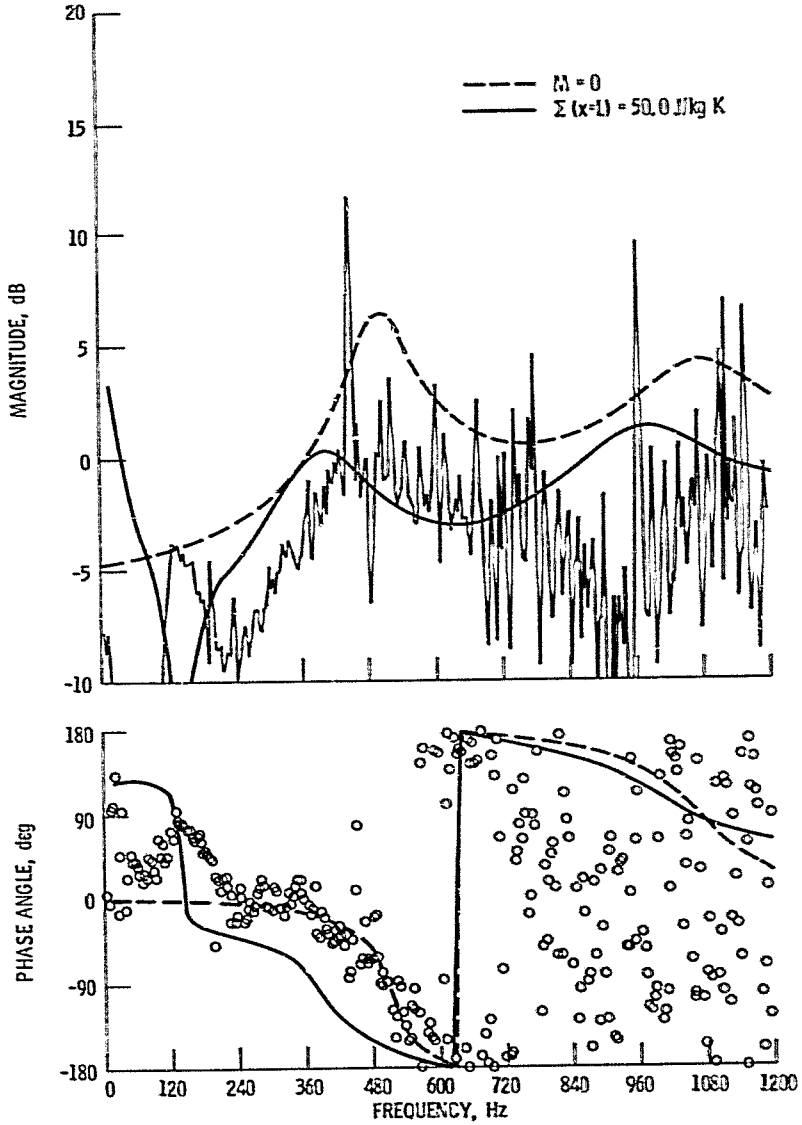

(d) JT15D nozzle transfer function 87%.

Figure 9. - Continued.

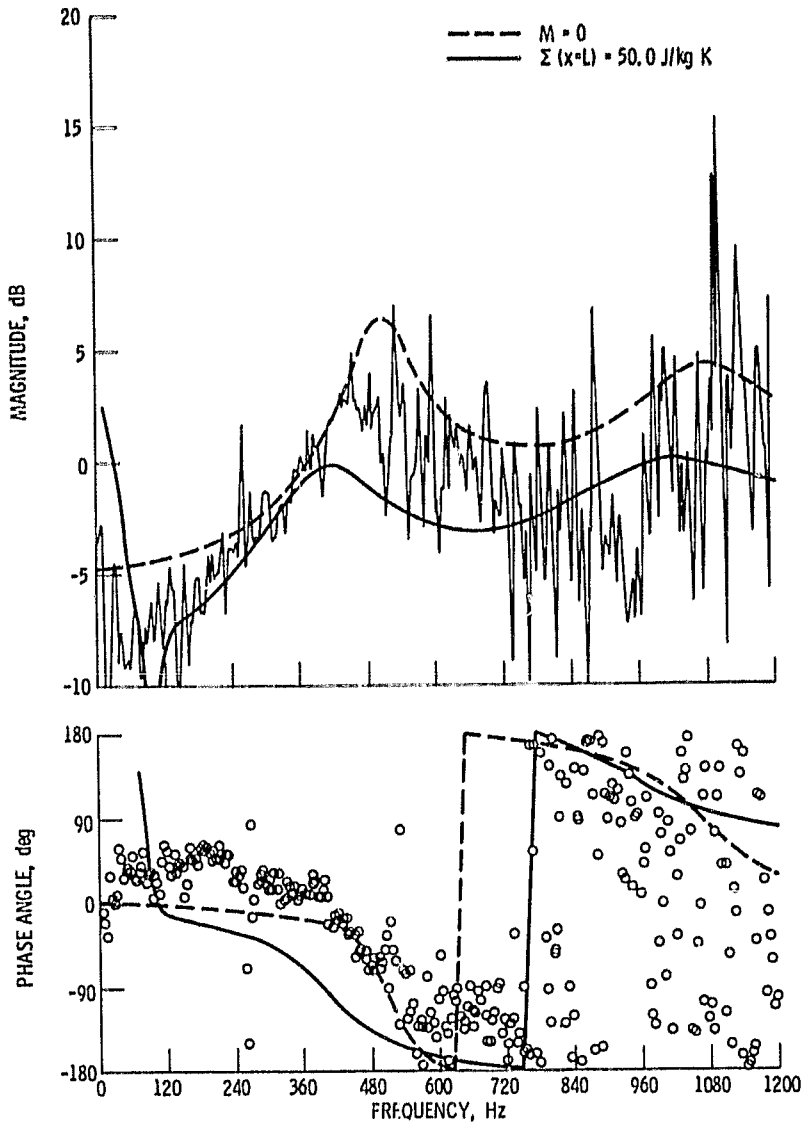

(e) JT15D nozzle transfer function 97 %.

Figure 9. - Concluded.